INTERNATIONAL JOURNAL FOR NUMERICAL METHODS IN FLUIDS, VOL. 25, 599–610 (1997)

NUMERICAL COMPUTATIONS OF INTERNAL FLOWS FOR AXISYMMETRIC AND TWO-DIMENSIONAL NOZZLES

S. S. GOKHALE* AND R. SURESH

Department of Aerospace Engineering, IIT, Madras 600 036, India

SUMMARY

MacCormack's explicit time-marching scheme is used to solve the full Navier–Stokes unsteady, compressible equations for internal flows. The requirement of a very fine grid to capture shock as well as separated flows is circumvented by employing grid clustering. The numerical scheme is applied for axisymmetric as well as two-dimensional flows. Numerical predictions are compared with experimental data and the qualitative as well as the quantitative agreement is found to be quite satisfactory. © 1997 by John Wiley & Sons, Ltd.

Int. J. Numer. Meth. Fluids, **25**: 599–610 (1997).

No. of Figures: 18. No. of Tables: 0. No. of References: 12.

KEY WORDS: axisymmetric nozzles; two-dimensional nozzles; Navier–Stokes solver; internal flows

INTRODUCTION

For the solution of the full Navier–Stokes equations as applicable to an actual complicated geometry, one can adopt various grid generation algorithms. For nozzle flows the viscous solution is able to predict internal flows over a wide Mach number range. These include flows with vortices such as found in secondary, wake or separated flows. Such flows are observed, for example, in the case of high-performance nozzles with larger expansion ratios or smaller radius of curvature at the throat, which need detailed fluid dynamic simulation for the accurate prediction of performance parameters.[1] This work deals with the numerical computation of nozzle flows for both two-dimensional and axisymmetric CFD nozzles for pressure ratios corresponding to full flow as well as separated flow.

The time-marching MacCormack two-step method is used to solve the Navier–Stokes equations.[2] This scheme is attractive because it is simple and does not require computations involving complicated matrix algebra. In addition, these methods could be easily modified for hardware-related parallel or vector codes or for complicated physical processes such as reactive chemistry or multiphase flows. However, these explicit methods do suffer from a longer computational time requirement. Some acceleration to convergence is possible with either local time stepping or a multigrid formulation.

* Correspondence to: S. S. Gokhale, Department of Aerospace Engineering, Indian Institute of Technology, Madras 600 036, India

CCC 0271–2091/97/050599–12 $17.50

Received November 1995
Revised October 1996

THEORETICAL MODEL

Nozzle flows can include shock–boundary layer interaction in and around the transonic region, entrance flow, exhaust wake flow and other flows which involve strong viscous–inviscid interactions with separated or reverse flow regions. For such cases it becomes necessary to solve the complete set of Navier–Stokes equations. The unsteady, compressible Navier–Stokes equations, which are a mixed set of hyperbolic–parabolic equations, can be written in the conservative form[3]

$$\frac{\partial \mathbf{U}}{\partial t}+\frac{\partial \mathbf{F}}{\partial x}+\frac{\partial \mathbf{G}}{\partial y}+\mathbf{H}=\mathbf{0},$$

where

$$\mathbf{U}=\begin{bmatrix}\rho\\ \rho u\\ \rho v\\ E_{\mathrm{t}}\end{bmatrix},\qquad \mathbf{F}=\begin{bmatrix}\rho u\\ \rho u^2+p-\tau_{xx}\\ \rho uv-\tau_{xy}\\ (E_{\mathrm{t}}+p)u-u\tau_{xx}-v\tau_{xy}+q_x\end{bmatrix},$$

$$\mathbf{G}=\begin{bmatrix}\rho v\\ \rho uv-\tau_{xy}\\ \rho v^2+p-\tau_{yy}\\ (E_{\mathrm{t}}+p)v-u\tau_{xy}-v\tau_{yy}+q_y\end{bmatrix},\qquad \mathbf{H}=\frac{I}{y}\begin{bmatrix}\rho v\\ \rho uv-\tau_{xy}\\ \rho v^2-(\tau_{yy}-\tau_{\theta\theta})\\ (E_{\mathrm{t}}+p)v-(u\tau_{xy}+v\tau_{yy}-q_y)\end{bmatrix},$$

with $I=0$ for 2D flows and $I=1$ for axisymmetric flows. The expressions for the viscosity and thermal conductivity include the corresponding turbulent terms

$$\mu=\mu_{\mathrm{l}}+\mu_{\mathrm{t}},\qquad k=\left(\frac{\mu_{\mathrm{l}}}{Pr_{\mathrm{l}}}+\frac{\mu_{\mathrm{t}}}{Pr_{\mathrm{t}}}\right)C_{\mathrm{p}}.$$

The Baldwin–Lomax turbulence model[4] is used to account for turbulence. This is an algebraic two-layer eddy viscosity model based on the Cebeci–Smith method, with a modification made to avoid having to locate the edge of the boundary layer. These governing equations are solved by the explicit finite difference scheme of MacCormack,[5] with the physical plane being mapped into a rectangular computational plane. This scheme is second-order- accurate in space and time. The forward and backward differencing can be alternated between predictor and corrector steps as well as between spatial derivatives in a sequential fashion to eliminate any bias due to one-sided differencing. A fine mesh is required in the viscous regions in order to resolve the boundary layer, whereas a coarser grid is used in the inviscid portion of the flow field. Roberts', stretching function,[6] which was later modified by Eiseman,[7] is given as

$$s=P\eta^*+(1-P)\left(1-\frac{\tanh[Q(1-\eta^*)]}{\tanh(Q)}\right),$$

where

$$\eta^*=\frac{\eta-\eta_{\mathrm{A}}}{\eta_{\mathrm{E}}-\eta_{\mathrm{A}}},\quad 0\leqslant\eta^*\leqslant 1.$$

P and Q are parameters which provide grid point control. P effectively provides the slope of the distribution and Q is a damping factor to control the departure from linearity. This grid clustering is employed in regions of large gradients such as the wall boundary, the throat and the approximate shock location in the case of separated flows.

In the present study, MacCormack's product fourth-order dissipation model[8] is employed to smooth the numerical oscillations associated with explicit schemes. This takes the form

$$\Delta U_{i,j} = C_x \frac{|P_{i+1,j} - 2P_{i,j} + P_{i-1,j}|(U_{i+1,j} - 2U_{i,j} + U_{i-1,j})(|U_{i,j}| + a_{i,j})\Delta t}{P_{i+1,j} - 2P_{i,j} + P_{i-1,j}}.$$

The quasi-one-dimensional initial data surface using a steady state area ratio–Mach number relation is prescribed as the initial condition. As the subsonic inlet boundary the stagnation pressure and stagnation temperature are fixed. For the supersonic exit flow, linear extrapolation is used, while for the subsonic exit flow the exit plane pressure is prescribed. The no-slip condition is assumed for the wall boundary. Wall pressures are obtained by solving the normal momentum equation. Wall temperatures are obtained for either adiabatic or isothermal conditions.

RESULTS AND DISCUSSION

Axisymmetric nozzles

JPL nozzle. Extensive data are available for the JPL nozzle and this nozzle was numerically simulated for validation of the existing numerical code. The computations are performed for the standard JPL nozzle with air at a stagnation pressure of 79 psia (482·62 kPa) and a temperature of 540°R (300 K) and compared with Cuffel *et al.*'s experimental data.[9]

In order to study the effect of grid refinement on the JPL nozzle, computations are performed for three different grid sizes, 40×25, 80×50 and 120×80, and the distribution of wall pressure–chamber pressure ratio is compared with the experimental results of Cuffel *et al.*[9] The comparison is shown in Figure 1. It is seen that with the fine grid the wall pressure predictions are qualitatively much better compared with the coarse grid, where the results are poor in the throat region owing to the larger grid spacing. In order to improve the solution in the throat region with the 40×25 grid, grid clustering in the throat region is carried out. The comparison of the 120×80 grid and the 40×25 grid with throat clustering is shown in Figure 2. As observed by Cuffel *et al.*,[9] the marginal static pressure

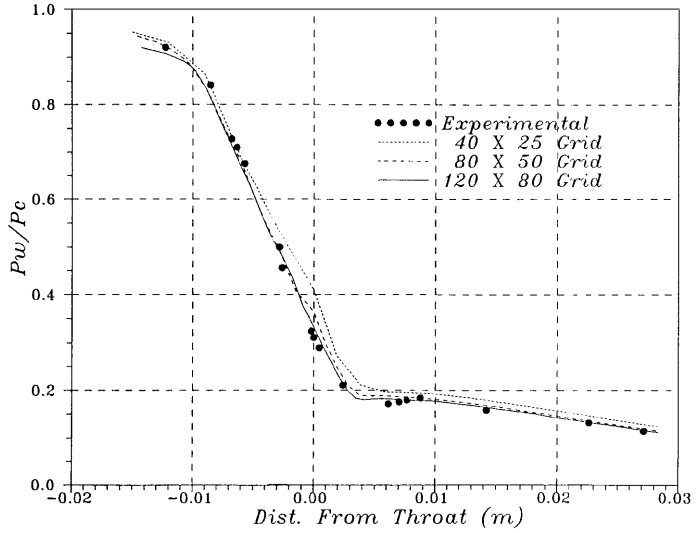

Figure 1. Wall pressure distribution as a function of grid size for JPL nozzle

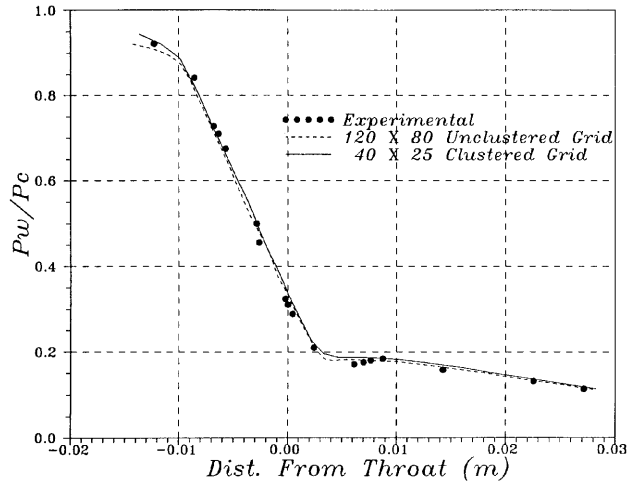

Figure 2. Wall pressure distribution for clustered and unclustered grids for JPL nozzle

rise along the wall just downstream of the tangency between the circular arc throat and the conical divergent section seen in Figures 1 and 2 is associated with a compressive turning of the flow. This is subsequently seen in Figure 3 in terms of converging and crowded iso-Mach lines. The essential features of the compressive turning shock are captured even for the 40×25 grid with clustering and are comparable with the numerical predictions with the 120×80 grid without clustering. It is observed that the clustered grid (40×25) computational time is an order of magnitude less compared with the unclustered fine grid (120×80).

The centreline Mach number distribution is compared with the experimental results in Figure 4. The experimental Mach number in the geometric throat plane is 0·8 at the axis and the predicted one is 0·79. The calculated flow coefficient of 0·986, defined as the ratio of the predicted to the one-dimensional mass flow rate, agrees well with the experimental value of 0·985. A Courant–Friedrich–Lewy number of 0·8 is utilized for all the calculations. The steady state is assumed to have been reached when the maximum error in the pressure has fallen by at least four orders of magnitude.

Results obtained by the current method are compared with the VNAP code for the calculation of compressible, viscous, internal flows.[2] Whereas the existing code requires 0·1 ms per grid per iteration, VNAP takes 0·075 ms per grid per iteration on a DEC Alpha workstation. The existing code

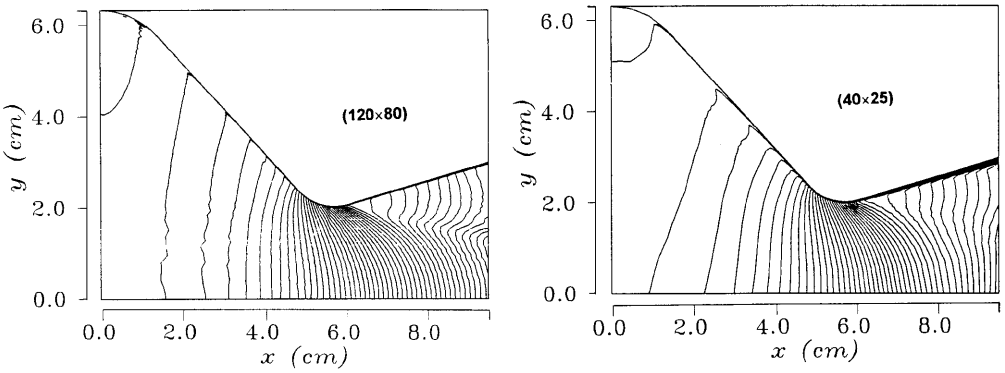

Figure 3. Iso-Mach contours for 120×80 unclustered and 40×25 clustered grids for JPL nozzle

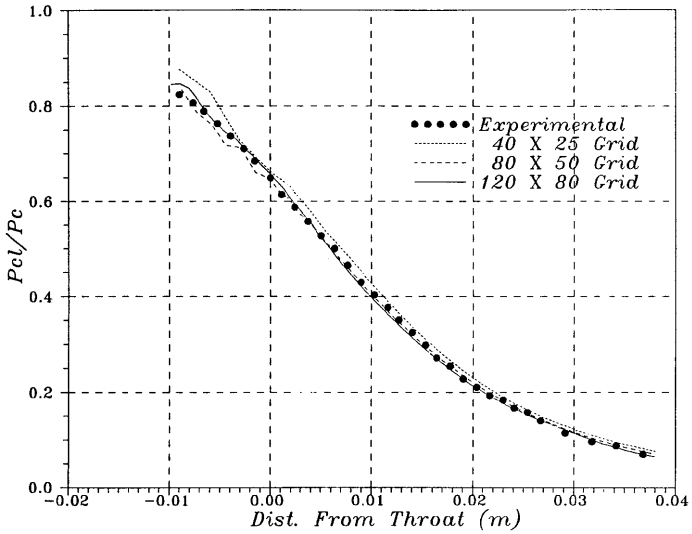

Figure 4. Centreline Mach number distribution as a function of grid size for JPL nozzle

performs the viscosity calculation every iteration, whereas VNAP assumes the viscosity to be constant, which can explain partially the time discrepancy. When the whole field is tested for convergence, VNAP needs about 3000 iterations, whereas the existing code needs nearly 5000 iterations. This is attributed to better boundary condition treatment in VNAP with the help of reference plane characteristics. Even though there is qualitative agreement between the two methods, the mass flow convergence of the existing code between the entrance, throat and exit regions is better compared with the VNAP code. Also the shock details are much better represented in the existing code. Even though there is not much difference between VNAP and the current code from the viewpoint of computer memory requirements, as would primarily be dictated by the number of conservation variables necessary for the computation as well as the array size, the current source code is about 60 per cent that of the VNAP code.

A2 nozzle.[10] This axisymmetric nozzle has half-angles of convergence and divergence of 15·69° and 4·25° respectively, and r_c/r_{th} of approximately 0·87 and an area ratio of 1·29. The computations are performed with a stagnation pressure–ambient pressure ratio of 6·2 and a stagnation temperature of 300 K for a grid size of 80×50 with clustering. Figure 5 gives the iso-Mach contours. The compressive turning shock is once again well captured. The predicted wall pressure distribution is compared with the experimental data in Figure 6. It is evident from this figure that there is reasonable qualitative agreement between experiment and theory. The computed mass flow rate and thrust are 2·35 kg s^{-1} and 1104 N respectively, whereas the corresponding experimental values are 2·25 kg s^{-1} and 1054 N.

Two-dimensional nozzles

Mason et al. nozzle.[11] The nozzle for which the results are presented here has an area ratio of 1·0891 and the Reynolds number based on stagnation conditions and throat half-height is $9{\cdot}3 \times 10^5$. The computations are performed with a grid size of 80×50. The only experimental data available for this nozzle were the wall pressure distribution shown in Figure 7. The predicted wall pressure

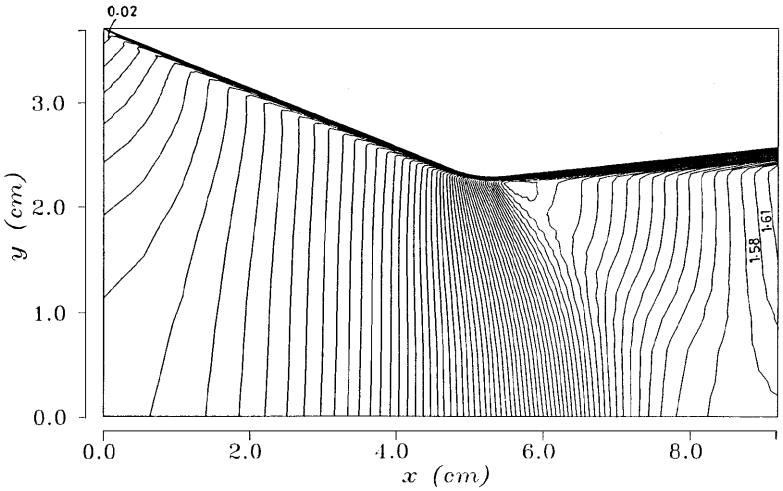

Figure 5. Iso-Mach contours for axisymmetric A2 nozzle (Arora)

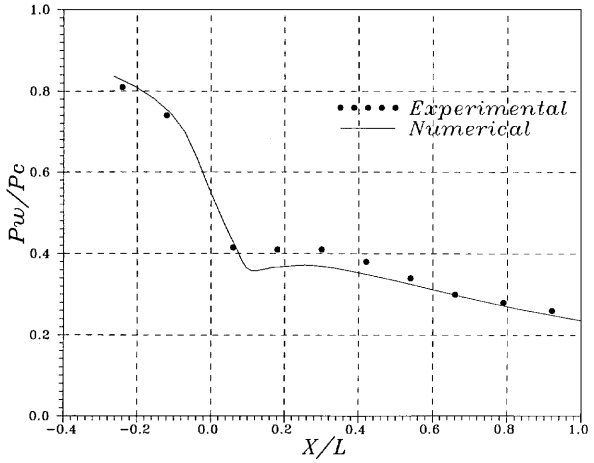

Figure 6. Comparison of experimental and numerical wall pressures for axisymmetric A2 nozzle (Arora)

distribution compared very well with the experimental data. Figure 8 shows the iso-Mach line pattern with boundary layer growth and wave reflection phenomena.

N5 nozzle.[10] More comprehensive experimental data are available for another two-dimensional nozzle having half-angles of convergence and divergence of 19·42° and 4·46° respectively, and r_c/r_{th} of approximately 0·93 and an area ratio of 1·49. The computations are performed for a pressure ratio of 5·97 and a temperature of 300 K with an 80×50 grid. Here again the predicted wall pressure distribution compares very well with the experimental data (Figure 9). The computed mass flow rate is 2·23 kg s^{-1} and the thrust is 992 N, whereas the experimental values are 2·12 kg s^{-1} and 1066 N respectively. The compressive turning shock (Figure 10) for this two-dimensional nozzle is not as pronounced as that for the axisymmetric nozzle, since there are only two surfaces with a sharper

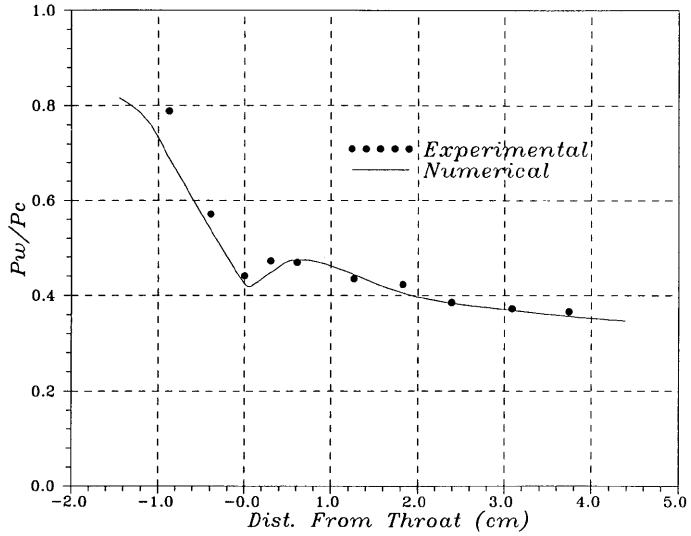

Figure 7. Comparison of experimental and numerical wall pressures for two-dimensional nozzle (Mason *et al.*)

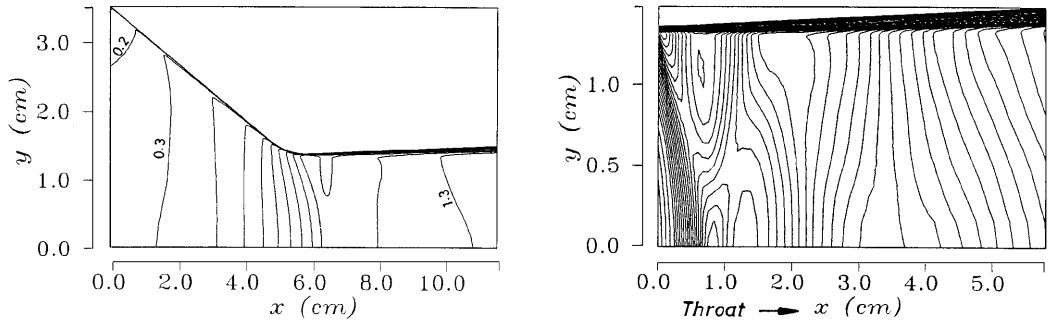

Figure 8. Iso-Mach contours for two-dimensional nozzle (Mason *et al.*)

radius of curvature at the throat, whereas the two remaining surfaces are straight ones which would not contribute to the coalescence of the pressure waves.

Separated nozzle flows

Chemical laser nozzle.[12] To study such a flow, computations are performed for an axisymmetric nozzle operating at a stagnation pressure of 6·895 kPa and a temperature of 289 K with a grid size of 80×30. The static pressure for all exit mesh points in the subsonic region is specified as 269 Pa. This plenum pressure causes the boundary layer to separate from the nozzle wall. Figure 11 shows the computed velocity field for the separated flow case. The recirculation zone associated with boundary layer separation is captured well by the present computations. Figure 12 shows the contour lines of constant Mach number for the separated case. There is reasonably good agreement with the experimental data for wall pressure distribution (Figure 13).

N5 nozzle.[10] These computations are performed for a 2D nozzle with a grid size of 60×25 and with grid clustering employed in the throat region and in the approximate normal shock location. The

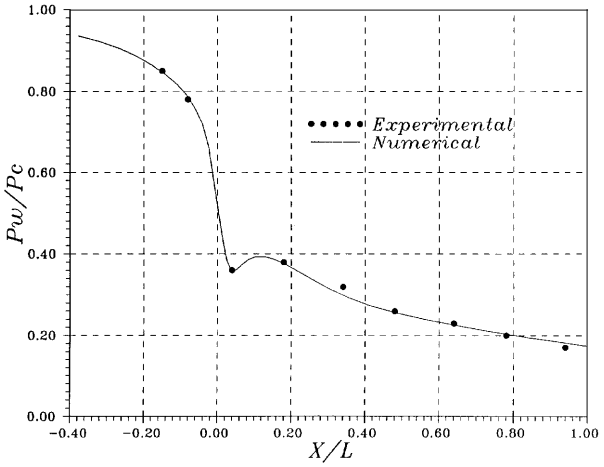

Figure 9. Comparison of experimental and numerical wall pressures for two-dimensional N5 nozzle (Arora)

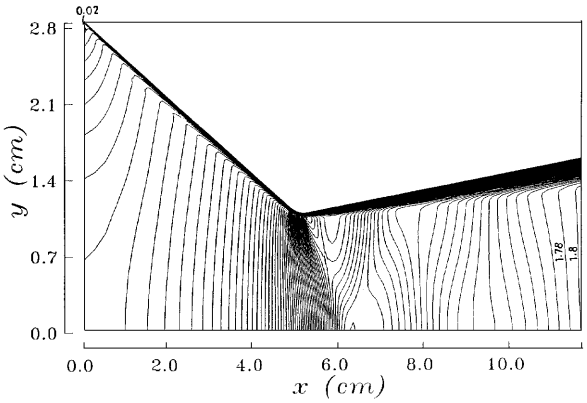

Figure 10. Iso-Mach contours for two-dimensional N5 nozzle (Arora)

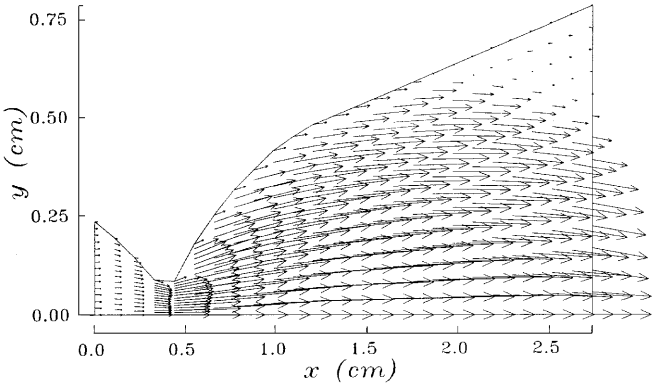

Figure 11. Velocity field in separated flow for axisymmetric nozzle (Hyde)

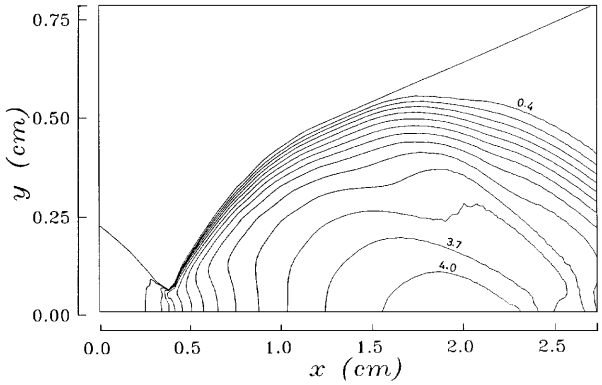

Figure 12. Iso-Mach contours for axisymmetric nozzle (Hyde)

pressure ratio p_c/p_a is kept as 2·01. The computed velocity field for the entire nozzle and for the separated flow region is shown in Figure 14. Figure 15 shows the computed Mach contours. The interaction between the shock wave and the boundary layer leads to the separation of the flow from the nozzle wall. The developed shear layer acts as a pseudo-throat and the subsonic flow after the shock accelerates and becomes supersonic through this throat. Figure 16 depicts multiple sonic lines for this case. Figure 17 shows the centreline Mach number distribution, which is obviously very different from the one for shock-free flow shown in Figure 4. The predicted wall pressure distribution shown in Figure 18 agrees extremely well with the experimental data. The measured mass flow rate is 0·707 kg s^{-1} and the computed one is 0·753 kg s^{-1}. The measured thrust is 182 N and the corresponding predicted value is 196·6 N. Since the pressure ratio is lower for the separated case, the values for the mass flow rate and thrust are much lower compared with the full flow. It is observed that it was not possible to capture such complex flow phenomena with the VNAP code.

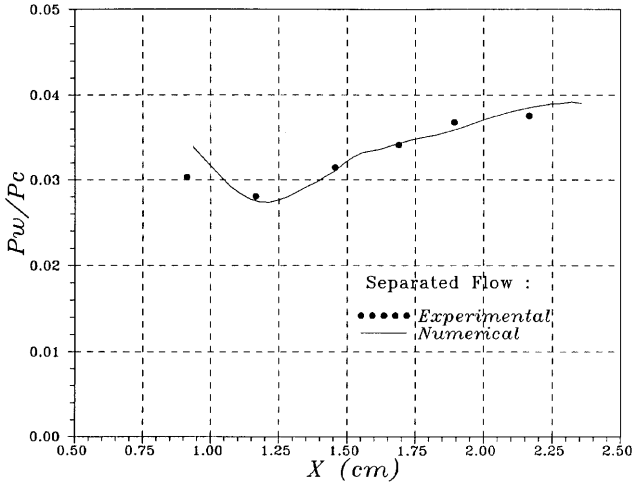

Figure 13. Comparison of experimental and numerical wall pressures for axisymmetric nozzle (Hyde)

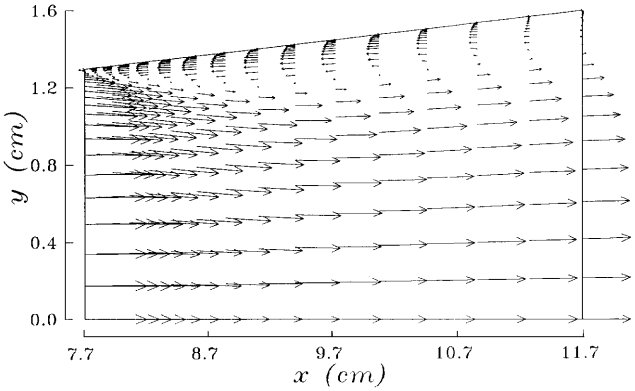

Figure 14. Velocity field in separated flow for two-dimensional N5 nozzle (Arora)

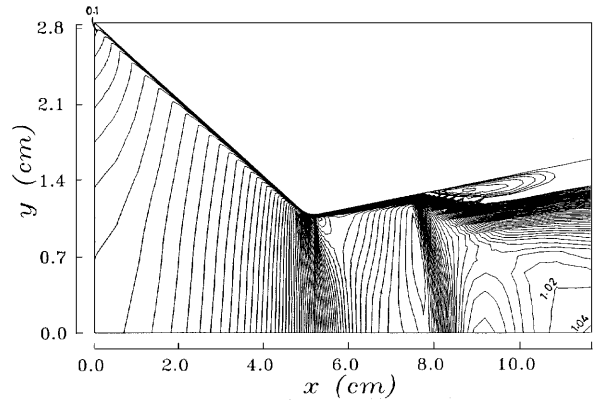

Figure 15. Iso-Mach contours for two-dimensional N5 nozzle (Arora)

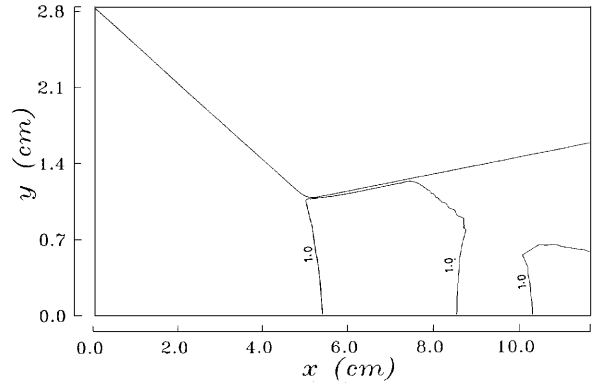

Figure 16. Multiple sonic lines for two-dimensional N5 nozzle (Arora)

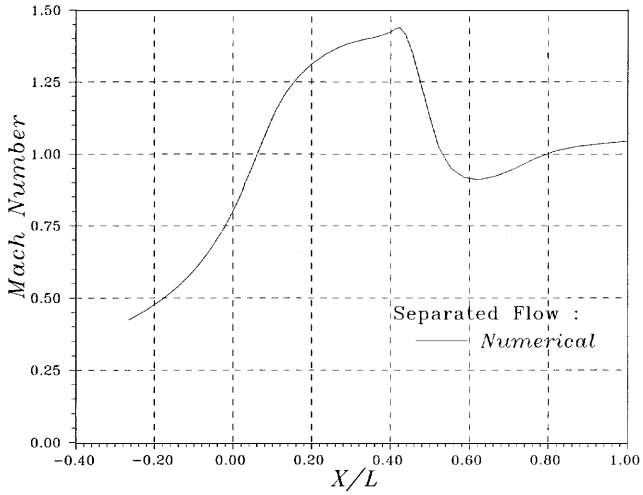

Figure 17. Centreline Mach number distribution for two-dimensional N5 nozzle (Arora)

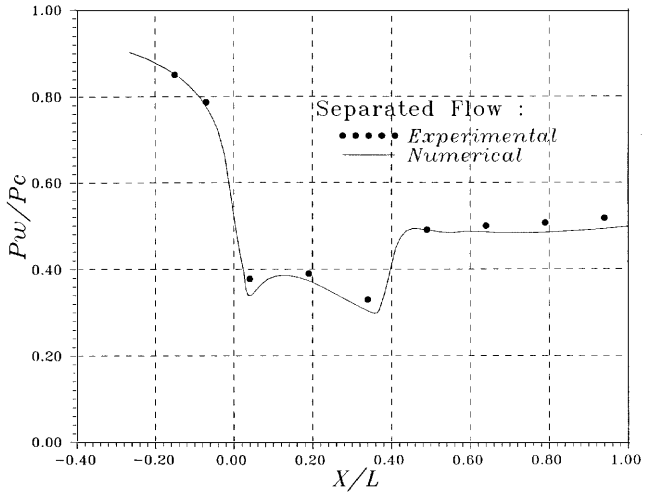

Figure 18. Comparison of experimental and numerical wall pressures for two-dimensional N5 nozzle (Arora)

CONCLUSIONS

An explicit finite difference code based on the full Navier–Stokes unsteady equations is developed to solve two-dimensional and axisymmetric internal flows using MacCormack's scheme along with algebraic grid clustering. It has been observed that the grid clustering allows faster steady state convergence in comparison with the unclustered grid, with much better details of the flow. The code was validated with the help of standard parameters measured experimentally, such as mass flow rate, thrust and wall pressures. There is good agreement, both qualitative and quantitative, between experiments and numerical predictions. Multiple wave reflection phenomena which could not be captured with the VNAP code were traceable with the existing code. The numerical predictions

provide additional insight with details about flow separation and reversal of flow as well as internal shocks and shock reflections.

REFERENCES

1. R. L. Davis, R. H. Ni and W. W. Bowley, 'Prediction of compressible, laminar viscous flows using a time-marching control volume and multiple-grid technique', *AIAA J.*, **22**, 1573–1581 (1984).
2. M. C. Cline, 'Computation of two-dimensional viscous nozzle flow', *AIAA J.*, **14**, 295–296 (1976).
3. Ch. Hirch, *Numerical Computation of Internal and External Flows*, Wiley, New York, 1988.
4. B. Baldwin and H. Lomax, 'Thin layer approximation and algebraic model for separated turbulent flows', *AIAA Paper 78-257*, 1978.
5. R. W. MacCormack, 'The effect of viscosity in hypervelocity impact cratering', *AIAA Paper 69-354*, 1969.
6. G. O. Roberts, 'Computational meshes for boundary layer problems', *Lect. Notes Phys.*, **8**, 171–177 (1971).
7. P. R. Eiseman, 'A multi-surface method of coordinate generation', *J. Comput. Phys.*, **33**, 118–150 (1979).
8. C. M. Hung and R. W. MacCormack, 'Numerical solutions of supersonic and hypersonic laminar compression corner flows', *AIAA J.*, **14**, 475–481 (1976).
9. R. F. Cuffel, L. H. Back and P. F. Masier, 'Transonic flowfield in a supersonic nozzle with small throat radius of curvature', *AIAA J.*, **7**, 1364–1366 (1969).
10. S. S. Gokhale and M. Arora, 'Experimental studies in axisymmetric and two-dimensional nozzles', *J. Aeronaut. Soc. India*, **48**, 207–220 (1996).
11. M. L. Mason, L. E. Putnam and R. J. Re, 'The effect of throat contouring on two-dimensional converging diverging nozzles at static conditions', *NASA TP 1704*, 1980.
12. J. C. Hyde, G. A. Hosac and G. S. Osugi, 'An investigation of velocity flowfields in chemical laser nozzles', *AIAA Paper 73-641*, 1973.

